

# Photostimulation for In Vitro Optogenetics with High-Power Blue Organic Light-Emitting Diodes

Andrew Morton, Caroline Murawski, Yali Deng, Changmin Keum, Gareth B. Miles, Javier A. Tello, and Malte C. Gather\*

Optogenetics, photostimulation of neural tissues rendered sensitive to light, is widely used in neuroscience to modulate the electrical excitability of neurons. For effective optical excitation of neurons, light wavelength and power density must fit with the expression levels and biophysical properties of the genetically encoded light-sensitive ion channels used to confer light sensitivity on cells—most commonly, channelrhodopsins (ChRs). As light sources, organic light-emitting diodes (OLEDs) offer attractive properties for miniaturized implantable devices for in vivo optical stimulation, but they do not yet operate routinely at the optical powers required for optogenetics. Here, OLEDs with doped charge transport layers are demonstrated that deliver blue light with good stability over millions of pulses, at powers sufficient to activate the ChR, CheRiff when expressed in cultured primary neurons, allowing live cell imaging of neural activity with the red genetically encoded calcium indicator, jRCaMP1a. Intracellular calcium responses scale with the radiant flux of OLED emission, when varied through changes in the current density, number of pulses, frequency, and pulse width delivered to the devices. The reported optimization and characterization of high-power OLEDs are foundational for the development of miniaturized OLEDs with thin-layer encapsulation on bioimplantable devices to allow single-cell activation in vivo.

Optogenetics is a versatile combination of light-sensitive molecular tools and photonics, which has transformed neuroscience by enabling light-mediated manipulations of cellular physiology.<sup>[1]</sup> The scope of the technique continues to expand through molecular engineering of microbial opsin genes,<sup>[2]</sup> transgenic and viral technologies for expressing opsins in neural tissues,<sup>[3]</sup> and innovations in the delivery of light to opsin-expressing cells.<sup>[4]</sup> Most studies use lasers or solid-state light-emitting diodes plus relay optics for optogenetic photostimulation, but the challenges presented by long-term in vivo studies and optogenetics-based visual and auditory neural prostheses are creating demand for novel photonic components.<sup>[5]</sup> Here, the feasibility of organic light-emitting diodes (OLEDs) as a lens-free method for photostimulation in optogenetics is demonstrated in vitro, laying a foundation for their incorporation in bioimplantable devices.

OLEDs are a distinct class of optical element contrasting with other light sources in design, because their emission emanates from a planar surface com-


prising a thin layer of an organic electroluminescent material sandwiched between two electrodes. Conceptually, this enables lens-free lab-on-chip designs since their thin structure allows OLEDs to be interfaced closely with biological samples without external relay optics. The emissive area of an OLED can have a wide range of physical scales, from millimeters or even centimeters (e.g., for sample illumination) to a few micrometers (to provide single-cell specificity and finely structured illumination).

OLEDs can be deposited on diverse substrates, including, importantly, active matrix backplanes (e.g., complementary metal oxide semiconductors (CMOS) or thin-film transistor arrays), to electrically address many pixels.<sup>[6]</sup> OLEDs can also be fabricated on lightweight flexible thin plastic films, offering opportunities for minimally invasive biocompatible implants.<sup>[7]</sup> Through engineering of the device electrodes, it is possible to design optically transparent OLEDs, which in the future may allow transillumination for imaging and microscopy. By selecting appropriate electroluminescent molecules, OLEDs can address the entire visible spectrum. Emissive layers of different colors can be stacked or spatially multiplexed to widen coverage of the spectrum from a single device.

Dr. A. Morton, Dr. C. Murawski, Y. Deng, Dr. C. Keum, Prof. M. C. Gather  
Organic Semiconductor Centre  
SUPA School of Physics and Astronomy  
University of St Andrews  
North Haugh KY16 9SS, St Andrews, UK  
E-mail: mcg6@st-andrews.ac.uk

Prof. G. B. Miles  
School of Psychology and Neuroscience  
University of St Andrews  
St Mary's Quad, South Street KY16 9JP, St Andrews, UK

Dr. J. A. Tello  
School of Medicine  
University of St Andrews  
Medical and Biological Sciences Building  
North Haugh KY16 9TF, St Andrews, UK

 The ORCID identification number(s) for the author(s) of this article can be found under <https://doi.org/10.1002/adbi.201800290>.

© 2019 The Authors. Published by WILEY-VCH Verlag GmbH & Co. KGaA, Weinheim. This is an open access article under the terms of the Creative Commons Attribution License, which permits use, distribution and reproduction in any medium, provided the original work is properly cited.

DOI: 10.1002/adbi.201800290

To date, work toward use of OLEDs for optogenetics has predominantly focused on light-sensitive biological model systems requiring low irradiances (power densities of the order of  $\mu\text{W mm}^{-2}$  or lower) to trigger their biological outputs. Blue-emitting OLED microdisplays with pixels of the size of biological cells and coated with thin-layer encapsulation (thickness,  $<1 \mu\text{m}$ ) to protect the OLED from the aqueous environment were used to drive phototactic behavior in *Chlamydomonas reinhardtii*<sup>[8]</sup> and to elicit single-cell activation of measurable photocurrents in human embryonic kidney cell lines expressing channelrhodopsins (ChRs) cultured directly on the devices.<sup>[9]</sup> In visual neuroscience, OLED microdisplays have been adopted to output visual stimuli onto isolated retinæ while making electrophysiological recordings, allowing detailed characterizations of visual receptive fields and functional connectivity between neurons of the retina.<sup>[10]</sup> Toward applications with higher irradiance requirements, millimeter-scale high-brightness OLEDs (operating in the range of  $0.25\text{--}0.4 \text{ mW mm}^{-2}$ ) were used to elicit ChR-triggered muscular contractions in vivo in *Drosophila* larvae.<sup>[11]</sup>

In the present study, the effectiveness of further-improved high-power millimeter-scale blue pin-OLEDs is evaluated in an all-optical system for stimulating and reading out neural activity in cultured neurons. We used blue-emitting pin-OLEDs with a bottom-emitting configuration (i.e., emitting through the glass substrate; **Figure 1a**; see the Experimental Section for details on OLED design and fabrication). Imaging chambers with primary cultures of mouse hippocampal neurons were placed on top of the OLED substrate and imaged with an upright microscope using a  $40\times/0.80 \text{ NA}$  water-dipping objective (**Figure 1b**). The active area of the OLEDs was  $16.36 \text{ mm}^2$  and illuminated the entire field of view. Like in earlier work on ChR-triggered muscular contractions in *Drosophila* larvae,<sup>[11]</sup> we used the fluorescent emitter material 2,5,8,11-tetra-*tert*-butylperylene (TBPe) to achieve good overlap of the OLED emission spectrum ( $\lambda_{\text{max}} = 463 \text{ nm}$ ) with the reported activation spectrum for CheRiff ( $\lambda_{\text{max}} \approx 460 \text{ nm}$ ),<sup>[12]</sup> a ChR with enhanced blue light sensitivity (**Figure 1c**). OLED electroluminescence and current density measurements (**Figure 1d**) indicated that a target optical power density of  $\approx 0.2 \text{ mW mm}^{-2}$ , previously reported to reliably trigger action potential firing in neurons expressing CheRiff,<sup>[12]</sup> was reached at modest driving voltages around  $5 \text{ V}$  (**Figure 1d**). Thus, OLED-mediated photostimulation of CheRiff expressed in cultured neurons was expected to generate measurable cellular responses. We also tested the stability of our OLEDs under high-brightness pulsed operation (optical power density,  $0.5 \text{ mW mm}^{-2}$ ; pulse duration,  $10 \text{ ms}$ ) and found that even after generating 1 million excitation pulses, the power density provided by our devices degraded by only about 20% indicating that these OLEDs likely have sufficient stability for extended in vivo experiments (**Figure 1e**).

Two recombinant adeno-associated virus (rAAV) vectors, one encoding CheRiff (tagged with eGFP) and the other encoding jRCaMP1a, a red genetically encoded calcium indicator (GECI), were used to transduce primary cultures of mouse hippocampal neurons. Robust expression, driven by a synapsin promoter, of both CheRiff-eGFP and jRCaMP1a was observed in most neurons from 1-week post-transduction onward. Confocal microscopy revealed that, qualitatively, expression patterns of both

vectors agreed well with their original descriptions,<sup>[12,13]</sup> with CheRiff-eGFP being highly membrane localized and jRCaMP1a being cytosolic and well exported from the nucleus (**Figure 2a**). Robust signal over background and a strong linear correlation between intensities of the two constructs were observed in neuronal cell bodies (**Figure 2b,c**). Signal intensities through the *z*-plane at neuronal cell bodies indicated that maximal CheRiff signal straddled cytosolic expression of jRCaMP1a outside the nucleus (**Figure 2d**). Collectively, these data verified that viral transduction with two rAAV vectors resulted in both CheRiff and jRCaMP1a being extensively coexpressed in our system and that they localized appropriately within neurons for optical stimulation and readout of neural activity.

Next, we interfaced the CheRiff- and jRCaMP1a-expressing neurons with OLEDs on a calcium imaging microscope setup and measured the neuronal responses to pulsed blue illumination from OLEDs (**Figure 1b**). We started by monitoring jRCaMP1a responses in neurons to a fixed train of 100 optical pulses from the OLED, with a duration of  $10 \text{ ms}$  each at  $80 \text{ Hz}$  (**Figure 3a,b**; Video S1, Supporting Information). Current densities between  $6$  and  $1125 \text{ mA cm}^{-2}$  were applied to the OLED, corresponding to optical power densities outputted by the OLED ranging from just under  $10 \mu\text{W mm}^{-2}$  to  $\approx 0.8 \text{ mW mm}^{-2}$ . Prior to optical stimulation, jRCaMP1a generated a clearly detectable and flat baseline of red fluorescence, indicating that the incident excitation light used for jRCaMP1a imaging did not cause significant CheRiff activation. During optical stimulation, the readout from cells was obscured by the emission of the OLED light bleeding through the  $600 \text{ nm}$  long-pass filter used for jRCaMP1a imaging. Immediately post-stimulation, significant increases in intracellular jRCaMP1a signal were recorded for all but the lowest optical power density tested and decayed with a half-decay time on the order of  $3 \text{ s}$ , consistent with the reported kinetics for jRCaMP1a in response to hundreds of action potentials.<sup>[13]</sup> At current densities below  $20 \text{ mA cm}^{-2}$  (corresponding to optical power densities incident on cells of less than  $10 \mu\text{W mm}^{-2}$ ), no neuronal responses were distinguishable above baseline noise levels (**Figure 3b,c**). At  $62.5 \text{ mA cm}^{-2}$  ( $\approx 60 \mu\text{W mm}^{-2}$  optical power density), peak signal/baseline jRCaMP1a responses immediately poststimulation reached  $0.08$  and approached a signal-to-noise (SNR) ratio of  $3\times$  the standard deviation (SD) of the baseline signal during the  $2 \text{ s}$  prior to stimulation (**Figure 3d**). Peak jRCaMP1a responses rapidly increased with increasing current densities, reaching signal/baseline of  $0.5$  and an  $\text{SNR} >20\times \text{SD}$  of baseline at  $750 \text{ mA cm}^{-2}$  ( $\approx 0.5 \text{ mW mm}^{-2}$ ). For even higher current densities, there was some tailing off in peak response amplitude, likely due to diminishing neuronal spike fidelity in response to photostimulation of CheRiff at higher frequencies.<sup>[12]</sup> Photostimulation-induced changes in jRCaMP1a signal were the result of CheRiff activation, since no detectable increases in jRCaMP1a signal were detected in matched neuronal cultures transduced with jRCaMP1a but not CheRiff (**Figure 3b**).

Next, we explored the minimum number of OLED light pulses that would elicit neuronal responses to photostimulation (again using  $10 \text{ ms}$  duration pulses at  $80 \text{ Hz}$  repetition rate and now using a fixed power density of  $0.8 \text{ mW mm}^{-2}$ ; **Figure 4a**). As expected, the amplitude of recorded neuronal jRCaMP1a responses increased as pulse trains of OLED photostimulation

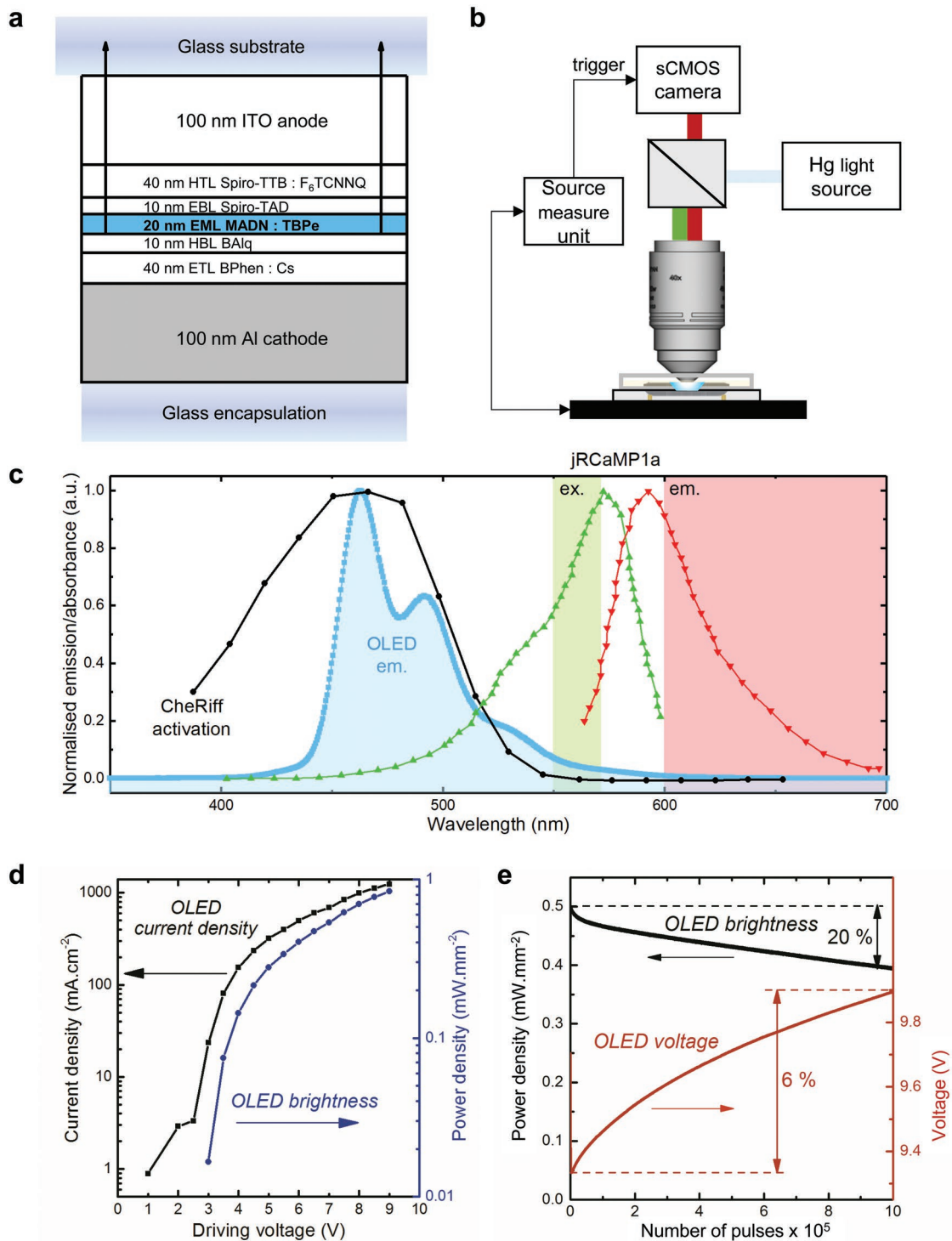


**Figure 1.** Properties of pin-OLEDs for in vitro optogenetics. a) OLED stack diagram, presented in the orientation in which devices were used in experiments (see the Experimental Section for details). b) Illustration of the optical setup used, incorporating bottom-emitting pin-OLED for optogenetic photostimulation and 40 $\times$ /0.80 NA water-dipping objective on an upright epifluorescence microscope configured for red GECI imaging. Image acquisition was triggered and OLED emission controlled by a source measure unit. c) Combined plot showing the measured OLED emission spectrum (blue squares), the activation spectrum of CheRiff<sup>[12]</sup> (black circles), and the excitation (ex.; green upward triangles) and emission (em.; red downward triangles) spectra of jRCaMP1a in the Ca<sup>2+</sup>-bound state.<sup>[13]</sup> Also shown are the excitation (green band) and emission (red band) wavelengths used for imaging jRCaMP1a responses. d) Current densities (black squares, left y-axis) and optical power densities (blue circles, right y-axis) measured for the 16.36 mm<sup>2</sup> OLED pixel. e) OLED stability under pulsed operation, applying 1 million constant-current pulses of 611 mA cm<sup>-2</sup> and 10 ms duration, with 10 Hz repetition rate. Optical power density (black line, left y-axis) generated during current pulses and corresponding bias voltage (red line, right y-axis).

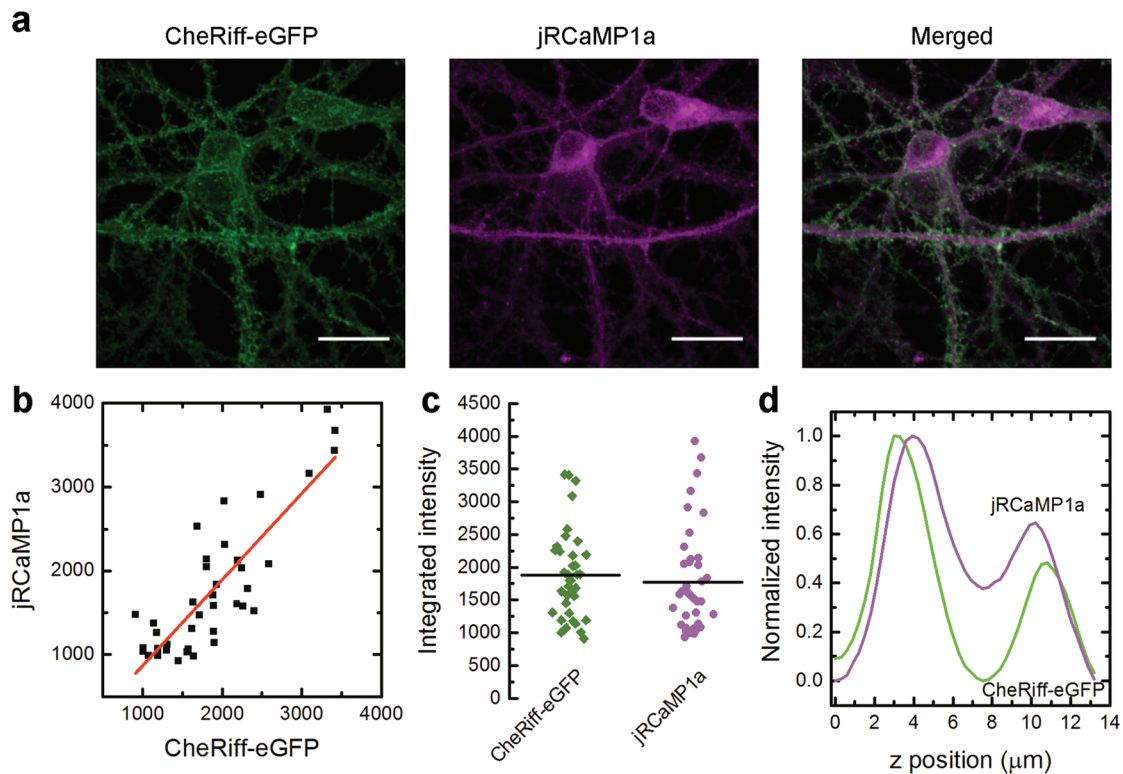


**Figure 2.** Coexpression of CheRiff and jRCaMP1a in cultured neurons transduced with rAAV vectors. a) Example fluorescence images of transduced neurons, from maximal projections of confocal z-stacks, pseudocolored with a green lookup table for CheRiff-eGFP and magenta for jRCaMP1a and shown as an overlay. Scale bars: 20  $\mu\text{m}$ . b) Linear fit to integrated intensities of jRCaMP1a against CheRiff-eGFP intensity at cell bodies ( $n = 39$  cells; Pearson correlation coefficient: 0.84). c) Distributions of integrated signal intensities for CheRiff-eGFP and jRCaMP1a in neuronal cell bodies as measured in part (b). Line indicates average. d) Average z-profiles from ROIs placed over the presumed nuclei in jRCaMP1a z-stacks of neurons ( $n = 10$  cells) to quantify the localization of CheRiff-eGFP and jRCaMP1a.

were lengthened to include more pulses. Ten pulses or more were required to generate jRCaMP1a responses statistically distinguishable from baseline noise levels, i.e., having an SNR of  $>3\times$  above the SD of the baseline signal; even a single excitation pulse produces an SNR slightly larger than 1 SD above baseline (Figure 4b,c).

To characterize calcium responses at less saturating stimulation frequencies and capture data between OLED pulses, we varied the duty cycle of OLED photostimulation. Figure 5a shows responses to 100 pulses, each 10 ms in duration, delivered at frequencies from 1 to 20 Hz (equating to duty cycles of 1–20%). Images acquired between OLED pulses delivered in this frequency range provided a readout of calcium summation during the period of OLED photostimulation. As was observed after stimulation with an individual pulse (Figure 4a), neuronal responses to each pulse within a 1 Hz pulse train were only marginally resolvable above the noise levels of the preceding prestimulus period. However, with successive pulses, the jRCaMP1a signal rapidly summated before reaching a steady-state signal/baseline of 0.15 after around 20 pulses. At higher photostimulation repetition rates of 5, 10, and 20 Hz, intracellular calcium continued to summate throughout the investigated stimulation period (Figure 5a).

Finally, at a fixed current ( $1125 \text{ mA cm}^{-2}$ ) and frequency (40 Hz) of stimulation, we varied the width of individual pulses within the pulse train between 1 and 20 ms. Photostimulation

with pulses of 1 and 3 ms substantially reduced the amplitude of jRCaMP1a signals measured immediately poststimulation (Figure 5b). Responses to 1 ms pulses were not distinguishable from noise levels but 3 ms pulses yielded signals above the threshold of detection in our system. The diminished responses to these shortened pulse widths are explained by the pulses being faster than the reported on-time of CheRiff (4.5 ms), i.e., the time over which CheRiff passes maximum photocurrents in hippocampal neurons.<sup>[12]</sup> Increasing the overall radiant flux by extending the pulse width to 20 ms (resulting in a duty cycle of 80%) resulted in jRCaMP1a responses with comparable amplitudes to stimulation at 80 Hz with 10 ms pulses.

Overall, these data show that it is feasible to use OLEDs for photostimulation in optogenetics and that their output is customizable to the fundamental biophysical properties of specific ChRs. Although well matched to the CheRiff activation spectrum, a potential limitation of our study is that the OLED emission overlaps with the jRCaMP1a fluorescence emission. Even though the overlap is small (OLEDs show  $<1\%$  relative emission at wavelengths  $>600 \text{ nm}$ ; Figure 1a), this precluded measurements of cellular jRCaMP1a signals during optical stimulation. Nonetheless, time-gated imaging permitted the recording of poststimulus neuronal calcium responses with ample temporal resolution for neuronal calcium dynamics and the dissociation kinetics of GECIs. Simultaneous OLED



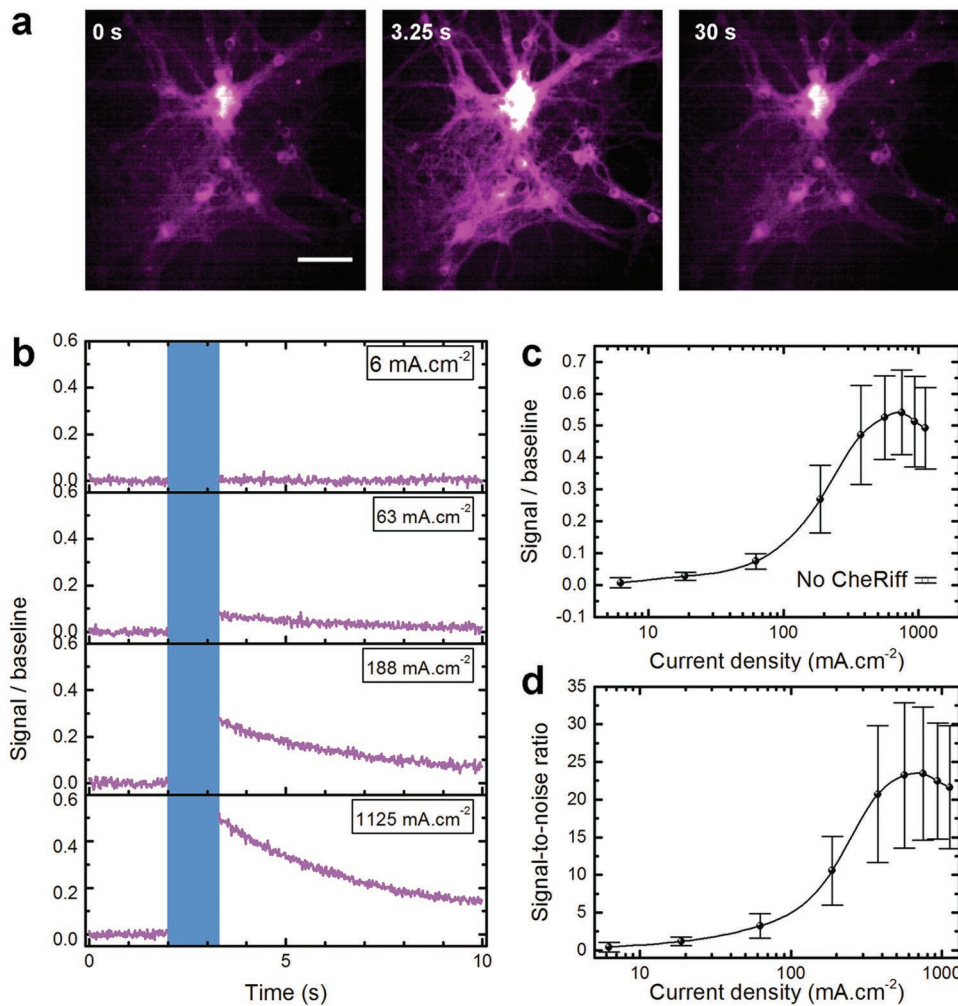


**Figure 3.** Responses of CheRiff-expressing neurons to OLED photostimulation at different current densities applied to the OLED. a) Individual frames from a representative jRCaMP1a calcium imaging time series before stimulation (0 s), immediately following OLED photostimulation (3.25 s), and 30 s after OLED photostimulation (30 s). Stimulation parameters: 100 pulses, each 10 ms in duration, delivered at 80 Hz, current density of  $1125 \text{ mA cm}^{-2}$  applied to OLED outputting an optical power density of  $\approx 0.8 \text{ mW mm}^{-2}$ . b) Mean jRCaMP1a responses (signal/baseline) of  $n = 10$  neurons to stimulation by OLED pulse train (blue bar) at different device current densities (indicated). Signal during OLED stimulation is omitted for clarity. c) jRCaMP1a signal/baseline as a function of current density at the OLED pixel (filled circles = mean, error bar = standard deviation,  $n = 10$  cells). Also shown (square symbol, no CheRiff) are measurements from cells transduced with jRCaMP1a but not CheRiff (current density  $1125 \text{ mA cm}^{-2}$ , symbol = mean, error bar = standard deviation,  $n = 10$  cells). d) jRCaMP1a signal-to-noise ratio as a function of current density of the OLED pixel (symbol = mean, error bar = standard deviation,  $n = 10$  cells).

stimulation and readout of neural excitation at temporal resolutions much higher than the imaging rate of  $50 \text{ s}^{-1}$  used here could deploy genetically encoded voltage indicator imaging, which typically operates at longer wavelengths,<sup>[12,14]</sup> or could record neuronal excitation using electrophysiology. Alternatively, the emission of OLEDs could be rendered more narrowband through introduction of a microcavity designed to selectively outcouple light at the desired wavelength.

Our work provides the basis for the future use of pin-OLEDs for lens-free in vivo photostimulation of neurons expressing ChRs, possibly with single-cell specificity. Due to the use of doped charge transport layers, the pin-OLEDs used here reach sufficient optical power density for photostimulation of ChR-expressing neurons at drive voltages below 5 V. This will

simplify integration of OLEDs for photostimulation of neurons on CMOS technology-based driver chips, which are often limited in their maximum available output voltage, but allow definition of OLED pixels with cell-scale dimensions, i.e., less than  $10 \mu\text{m} \times 10 \mu\text{m}$ . The low driving voltage also reduces ohmic losses in the OLED, thus minimizing potentially adverse device heating. Continued refinements in molecular engineering now enable restricted expression of ChRs to neuronal cell bodies, a critical step in avoiding aberrant activation of distant cells via activation of en-passant ChR-expressing axons and dendrites.<sup>[15]</sup> In combination, these developments open the future possibility of a microscopic version of the high-brightness OLEDs used here to enable lens-free yet single-cell-specific photostimulation.

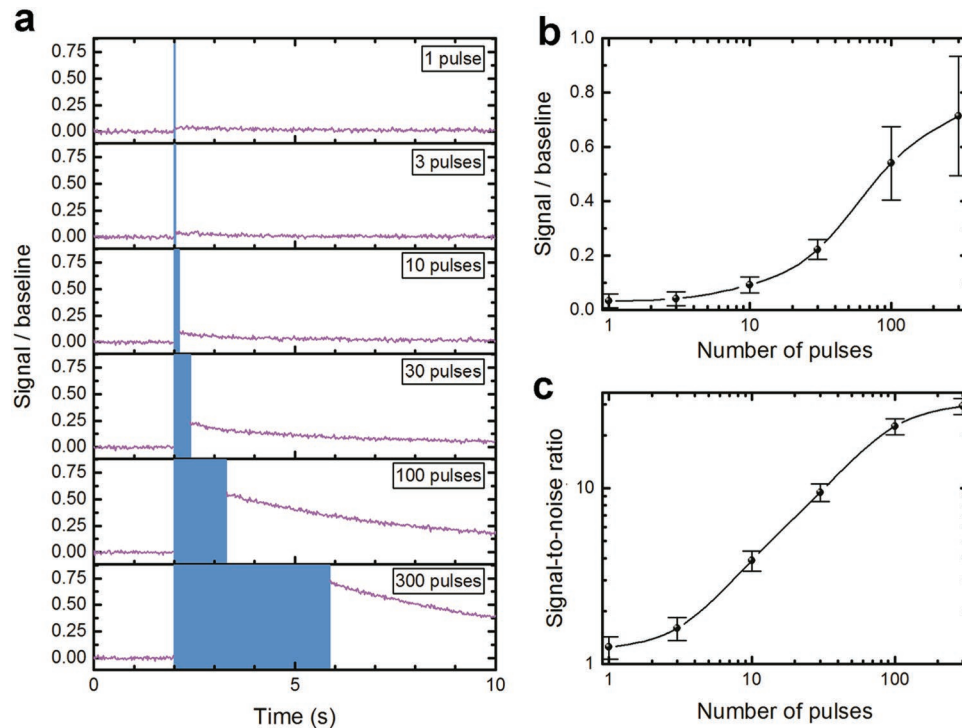


**Figure 4.** Sensitivity threshold of neuronal responses to varying numbers of OLED pulses. a) Signal/baseline jRCaMP1a mean traces ( $n = 10$  cells) for the indicated number of pulses of OLED photostimulation (stimulation parameters: 10 ms duration pulses, delivered at 80 Hz, current density of  $1125 \text{ mA cm}^{-2}$  outputting roughly  $0.8 \text{ mW mm}^{-2}$ ). b) jRCaMP1a signal/baseline as a function of the number of pulses of OLED photostimulation (symbol = mean, error bar = standard deviation,  $n = 10$  cells). c) jRCaMP1a SNR as a function of the number of pulses of OLED photostimulation (symbol = mean, error bar = standard deviation,  $n = 10$  cells).

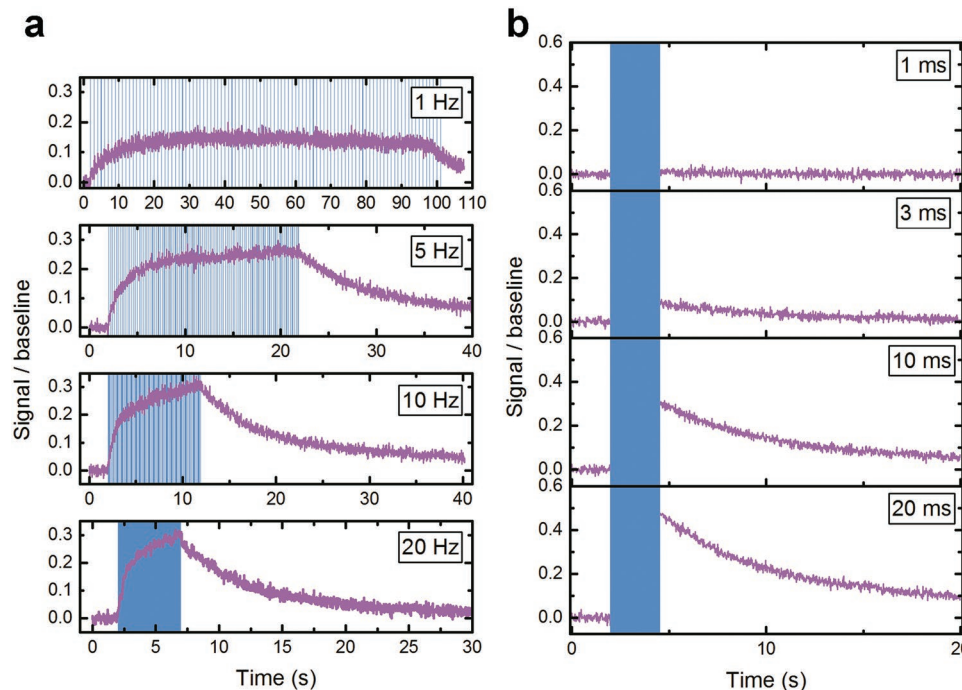


**Figure 5.** Neuronal calcium responses to varying duty cycles of OLED photostimulation. a) jRCaMP1a signal/baseline traces (purple lines: mean response from  $n = 10$  cells) in response to OLED photostimulation (blue bars) at different repetition rates. Stimulation parameters: 100 pulses, 10 ms duration, OLED pixel current density  $1125 \text{ mA cm}^{-2}$ , optical power density  $0.8 \text{ mW mm}^{-2}$ , delivered at the indicated repetition rates. b) Mean jRCaMP1a signal/baseline traces (purple lines,  $n = 10$  cells) in response to OLED photostimulation with trains containing pulses of different widths. Stimulation parameters: 100 pulses, repetition rate 40 Hz, current density at OLED pixel  $1125 \text{ mA cm}^{-2}$ , optical power density  $0.8 \text{ mW mm}^{-2}$ , pulse width as indicated.

## Experimental Section

**OLED Fabrication and Characterization:** OLEDs were fabricated in a high-vacuum chamber (Angstrom Engineering) at a base pressure of  $10^{-7}$  mbar. All materials were purchased from commercial suppliers. Organic materials were evaporated sequentially onto glass substrates coated with a prestructured indium tin oxide (ITO) anode. ITO anode length connecting to the OLED pixel was reduced from 4 mm in initial devices (Figure 1e) to less than 1 mm for devices used in optogenetic experiments (Figure 1d). Layer thickness was monitored in situ using quartz crystal monitors. Devices were composed of the following layers of materials: hole transport layer, thickness: 40 nm, 2,2',7,7'-tetrakis(*N,N'*-di-*p*-methylphenylamino)-9,9'-spirobifluorene *p*-doped with 2,2'-(perfluoronaphthalene-2,6-diylidene)dimalononitrile (4 wt%); electron blocking layer, thickness: 10 nm, 2,2',7,7'-tetrakis(*N,N'*-diphenylamino)-9,9'-spirobifluorene; emission layer, thickness: 20 nm, TBPe doped at 1.5 wt% into the host 2-methyl-9,10-bis(naphthalen-2-yl)anthracene; hole blocking layer, thickness: 10 nm, bis(2-methyl-8-quinolinolate)-(4-phenylphenolato)aluminum(III); electron transport layer, thickness: 40 nm, cesium-doped 4,7-diphenyl-1,10-phenanthroline (3 wt%); cathode, thickness: 100 nm, aluminum. OLEDs were fabricated in one run using shadow masks and subsequently encapsulated under nitrogen atmosphere using glass lids and epoxy resin. Each substrate contained four identical OLEDs with an active area of 16.36 mm<sup>2</sup>.

**Primary Culture and Viral Transduction of Neurons:** All animal care and procedures were in accordance with the United Kingdom Animals (Scientific Procedures) Act 1986 and animals culled by Schedule 1 methods. Hippocampi from unsexed postnatal day 2–3 C57BL/6 laboratory mouse pups were dissected and pooled in ice-cold DPBS. Tissue was treated with papain (10 units mL<sup>-1</sup>) for 22 min at 37 °C and then disaggregated by repeated pipetting in Dulbecco's modified Eagle medium/nutrient mixture F-12 containing 10% fetal bovine serum. Cells were pelleted by centrifugation for 5 min at 200 × *g* and resuspended in culture medium (Neurobasal-A supplemented with B-27 and  $0.5 \times 10^{-3}$  M GlutaMax-I). Cells were then seeded at a nominal initial density of 400 cells mm<sup>-2</sup> on polyornithine and laminin-coated 10 mm diameter glass coverslips housed in 24-well plates maintained in a humidified incubator at 37 °C and 5% CO<sub>2</sub>. At 4–7 d in vitro, cultures were transduced with independent rAAV particle preparations packaging CheRiff<sup>[12]</sup> and jRCaMP1a<sup>[13]</sup> ( $2 \times 10^9$  gc per coverslip) while performing a 50% volume change of culture medium. DRH337:AAV-hsyn-CheRiff-eGFP was a gift from Adam Cohen (Addgene plasmid # 51697). AAV1/2 particles of hsyn-CheRiff-eGFP were produced in HEK cells and concentrated by heparin column purification.<sup>[16]</sup> AAV1 virions for jRCaMP1a (AAV1.Syn.NES.jRCaMP1a.WPRE.SV40) were prepared by the University of Pennsylvania Vector Core.

**OLED and Live Cell Imaging Setup:** OLEDs were mounted in a custom sample holder on the stage of an upright microscope and connected electrically to a source measure unit (SMU Keithley 2450). Incident light for imaging jRCaMP1a was from a fiber-coupled mercury arc lamp attenuated with neutral-density filters and filtered 560/20 nm. Emission was collected above 600 nm on an sCMOS camera (Andor Neo) at 50 s<sup>-1</sup> with 8 × 8 pixel binning through a 40x/0.80 NA water-dipping objective. Electrical control of OLEDs was performed using Python scripts to program the SMU: a trigger pulse was sent from the SMU to initiate acquisition from the camera for 2 s and then deliver constant-current pulse trains to the OLEDs with varied currents, pulse widths, numbers of pulses, and pulse frequency, as described in the text. Experiments were performed at room temperature (20–22 °C). The bath solution for imaging was 125 × 10<sup>-3</sup> M NaCl, 2.5 × 10<sup>-3</sup> M KCl, 3 × 10<sup>-3</sup> M CaCl<sub>2</sub>, 1 × 10<sup>-3</sup> M MgCl<sub>2</sub>, 10 × 10<sup>-3</sup> M HEPES, and 30 × 10<sup>-3</sup> M glucose, pH 7.3. Experiments were performed under pharmacological blockade of AMPA, kainate, and NMDA receptors with 10 × 10<sup>-6</sup> M CNQX and 25 × 10<sup>-6</sup> M d-APV, since optical stimulation triggered recurrent network activity in untreated cultures.

**Image Analysis:** Raw image sequences from calcium imaging were exported to a Fiji ImageJ distribution for analysis.<sup>[17]</sup> Identically sized regions of interest (ROIs) were placed over manually identified neuronal

cell bodies using the Time Series Analyzer plug-in. Mean pixel intensity within each of these ROIs was then calculated for each frame. To normalize traces for variation in basal fluorescence levels, traces are presented as signal/baseline, where signal is the difference between fluorescence at any given time point and the average fluorescence within the 100 frames (2 s) acquired before the OLED stimulus (baseline). The signal/baseline data are thus comparable to a  $\Delta F/F_0$  value, except that the baseline averaging reduces noise vs using only a single initial point in time as is sometimes implied by the term  $F_0$ . Where individual signal/baseline values are presented, these are the average signal from the five frames immediately post-OLED stimulation. Where signal-to-noise ratio is presented, signal is defined as above, with noise being calculated as the standard deviation of pixel intensity values during the 100 frames (2 s) before stimulation.

**Data Availability:** The research data supporting this publication can be accessed at <https://doi.org/10.17630/80cbac70-227e-4564-9a8c-937257e9c49d>.

## Supporting Information

Supporting Information is available from the Wiley Online Library or from the author.

## Acknowledgements

The authors are grateful for financial support from the Leverhulme Trust (RPG-2017-231), the EPSRC NSF-CBET lead agency agreement (EP/R010595/1, 1706207), the DARPA NESD program (N66001-17-C-4012), and the RS Macdonald Charitable Trust. C.M. acknowledges funding by the European Commission through a Marie Skłodowska-Curie Individual Fellowship (703387). Y.D. acknowledges support from the Chinese Scholarship Council.

## Conflict of Interest

The authors declare no conflict of interest.

## Keywords

channelrhodopsin, optogenetics, organic light-emitting diodes, photostimulation

Received: October 18, 2018

Revised: December 14, 2018

Published online:

[1] K. Deisseroth, *Nat. Neurosci.* **2015**, *18*, 1213.

[2] a) J. Mattis, K. M. Tye, E. A. Ferenczi, C. Ramakrishnan, D. J. O'Shea, R. Prakash, L. A. Gunaydin, M. Hyun, L. E. Fenno, V. Gradinaru, O. Yizhar, K. Deisseroth, *Nat. Methods* **2012**, *9*, 159; b) F. Zhang, J. Vierock, O. Yizhar, L. E. Fenno, S. Tsunoda, A. Kianianmomeni, M. Prigge, A. Berndt, J. Cushman, J. Polle, J. Magnuson, P. Hegemann, K. Deisseroth, *Cell* **2011**, *147*, 1446; c) N. C. Klapoetke, Y. Murata, S. S. Kim, S. R. Pulver, A. Birdsey-Benson, Y. K. Cho, T. K. Morimoto, A. S. Chuong, E. J. Carpenter, Z. Tian, J. Wang, Y. Xie, Z. Yan, Y. Zhang, B. Y. Chow, B. Surek, M. Melkonian, V. Jayaraman, M. Constantine-Paton, G. K. Wong, E. S. Boyden, *Nat. Methods* **2014**, *11*, 338.

[3] a) L. Madisen, T. Mao, H. Koch, J. M. Zhuo, A. Berenyi, S. Fujisawa, Y. W. Hsu, A. J. Garcia 3rd, X. Gu, S. Zanella, J. Kidney, H. Gu,

- Y. Mao, B. M. Hooks, E. S. Boyden, G. Buzsaki, J. M. Ramirez, A. R. Jones, K. Svoboda, X. Han, E. E. Turner, H. Zeng, *Nat. Neurosci.* **2012**, *15*, 793; b) T. L. Daigle, L. Madisen, T. A. Hage, M. T. Valley, U. Knoblich, R. S. Larsen, M. M. Takeno, L. Huang, H. Gu, R. Larsen, M. Mills, A. Bosma-Moody, L. A. Siverts, M. Walker, L. T. Graybeck, Z. Yao, O. Fong, T. N. Nguyen, E. Garren, G. H. Lenz, M. Chavarha, J. Pendergraft, J. Harrington, K. E. Hirokawa, J. A. Harris, P. R. Nicovich, M. J. McGraw, D. R. Ollerenshaw, K. A. Smith, C. A. Baker, J. T. Ting, S. M. Sunkin, J. Lecoq, M. Z. Lin, E. S. Boyden, G. J. Murphy, N. M. da Costa, J. Waters, L. Li, B. Tasic, H. Zeng, *Cell* **2018**, *174*, 465.
- [4] A. M. Packer, B. Roska, M. Hausser, *Nat. Neurosci.* **2013**, *16*, 805.
- [5] a) J. M. Barrett, R. Berlinguer-Palmini, P. Degenaar, *Visual Neurosci.* **2014**, *31*, 345; b) T. Mager, D. Lopez de la Morena, V. Senn, J. Schlotte, A. D'Errico, K. Feldbauer, C. Wrobel, S. Jung, K. Bodensiek, V. Rankovic, L. Browne, A. Huet, J. Juttner, P. G. Wood, J. J. Letzkus, T. Moser, E. Bamberg, *Nat. Commun.* **2018**, *9*, 1750; c) C. Wrobel, A. Dieter, A. Huet, D. Keppeler, C. J. Duque-Afonso, C. Vogl, G. Hoch, M. Jeschke, T. Moser, *Sci. Transl. Med.* **2018**, *10*, eaao0540
- [6] J. K. Jeong, *Semicond. Sci. Technol.* **2011**, *26*, 034008.
- [7] M. S. White, M. Kaltenbrunner, E. D. Głowacki, K. Gutnichenko, G. Kettlgruber, I. Graz, S. Aazou, C. Ulbricht, D. A. M. Egbe, M. C. Miron, Z. Major, M. C. Scharber, T. Sekitani, T. Someya, S. Bauer, N. S. Sariciftci, *Nat. Photonics* **2013**, *7*, 811.
- [8] A. Steude, M. Jahnel, M. Thomschke, M. Schober, M. C. Gather, *Adv. Mater.* **2015**, *27*, 7657.
- [9] A. Steude, E. C. Witts, G. B. Miles, M. C. Gather, *Sci. Adv.* **2016**, *2*, e1600061.
- [10] a) J. Johnston, L. Lagnado, *eLife* **2015**, *4*, 06250; b) J. Johnston, H. Ding, S. H. Seibel, F. Esposti, L. Lagnado, *J. Physiol.* **2014**, *592*, 4839.
- [11] A. Morton, C. Murawski, S. R. Pulver, M. C. Gather, *Sci. Rep.* **2016**, *6*, 31117.
- [12] D. R. Hochbaum, Y. Zhao, S. L. Farhi, N. Klapoetke, C. A. Werley, V. Kapoor, P. Zou, J. M. Kralj, D. Maclaurin, N. Smedemark-Margulies, J. L. Saulnier, G. L. Boulting, C. Straub, Y. K. Cho, M. Melkonian, G. K. Wong, D. J. Harrison, V. N. Murthy, B. L. Sabatini, E. S. Boyden, R. E. Campbell, A. E. Cohen, *Nat. Methods* **2014**, *11*, 825.
- [13] H. Dana, B. Mohar, Y. Sun, S. Narayan, A. Gordus, J. P. Hasseman, G. Tsegaye, G. T. Holt, A. Hu, D. Walpita, R. Patel, J. J. Macklin, C. I. Bargmann, M. B. Ahrens, E. R. Schreiter, V. Jayaraman, L. L. Looger, K. Svoboda, D. S. Kim, *eLife* **2016**, *5*, e12727.
- [14] K. D. Piatkevich, E. E. Jung, C. Straub, C. Linghu, D. Park, H. J. Suk, D. R. Hochbaum, D. Goodwin, E. Pnevmatikakis, N. Pak, T. Kawashima, C. T. Yang, J. L. Rhoades, O. Shemesh, S. Asano, Y. G. Yoon, L. Freifeld, J. L. Saulnier, C. Riegler, F. Engert, T. Hughes, M. Drobizhev, B. Szabo, M. B. Ahrens, S. W. Flavell, B. L. Sabatini, E. S. Boyden, *Nat. Chem. Biol.* **2018**, *14*, 352.
- [15] a) O. A. Shemesh, D. Tanese, V. Zampini, C. Linghu, K. Piatkevich, E. Ronzitti, E. Papagiakoumou, E. S. Boyden, V. Emiliani, *Nat. Neurosci.* **2017**, *20*, 1796; b) A. R. Mardinly, I. A. Oldenburg, N. C. Pegard, S. Sridharan, E. H. Lyall, K. Chesnov, S. G. Brohawn, L. Waller, H. Adesnik, *Nat. Neurosci.* **2018**, *21*, 881.
- [16] C. McClure, K. L. H. Cole, P. Wulff, M. Klugmann, A. J. Murray, *J. Visualized Exp.* **2011**, *57*, e3348.
- [17] a) J. Schindelin, I. Arganda-Carreras, E. Frise, V. Kaynig, M. Longair, T. Pietzsch, S. Preibisch, C. Rueden, S. Saalfeld, B. Schmid, J. Y. Tinevez, D. J. White, V. Hartenstein, K. Eliceiri, P. Tomancak, A. Cardona, *Nat. Methods* **2012**, *9*, 676; b) C. A. Schneider, W. S. Rasband, K. W. Eliceiri, *Nat. Methods* **2012**, *9*, 671.